Object-based evaluation of precipitation systems in convection-permitting regional climate simulation over eastern China

Ziyue Guo[1,2], Jianping Tang[1,2], Jie Tang[3], Juan Fang[1,2], Wei Luo[4]

1. Key Laboratory of Mesoscale Severe Weather/Ministry of Education, Nanjing University, Nanjing, 210023, China

2. School of Atmospheric Sciences, Nanjing University, Nanjing, 210023, China

3. Shanghai Typhoon Institute, China Meteorological Administration, Shanghai, China

4. Department of Computer Science and Technology, Nanjing University, Nanjing, 210023, China

Corresponding Author: Juan Fang, School of Atmospheric Sciences, Nanjing University, 163 Xianlin Road, Nanjing, China. Email: fangjuan@nju.edu.cn

Submitted to: JGR-Atmospheres

Key Points:

- General properties of precipitation systems are analyzed in long-term convection-permitting simulations over eastern China.
- Precipitation systems are substantially too intense but with the limited coverage area in convection-permitting simulations.
- Wet biases and dry biases for shorter-duration and longer-duration systems can be reduced by using spectral nudging at convection-permitting scale.

Abstract

Based on the object-based tracking algorithm, the precipitation simulation ability of the convection-permitting (CP) regional climate models (RCMs) is evaluated from the viewpoints of the precipitation systems in this work. The characteristics of precipitation systems over eastern China during 1998-2007 derived from the Weather Research and Forecasting model (WRF) with the horizontal grid spacing of ~ 4 km are compared with CMORPH. On the whole, CP RCMs can capture the average duration and eccentricity of all precipitation systems reasonably. However, precipitation systems tend to be stronger but with smaller coverage area in CP RCMs, which leads to the wet biases and dry biases of accumulated precipitation amount in the longer-duration (>= 48 hr) and shorter-duration (< 48 hr) systems, respectively. Such deficiencies in accumulated precipitation amount of precipitation systems with various durations can be made up by employing spectral nudging technique in CP RCMs to a certain degree. This work further indicates that, to improve the capability of precipitation simulation in CP RCMs, the relationship between intensity and coverage area of precipitation systems should be described properly in CP RCMs, especially for those with shorter-duration.

Key words: Convection-permitting; Regional climate model; Precipitation system; Objected-

based algorithm; Spectral nudging

1. Introduction

Precipitation is the most challenging climate variables to regional climate models (RCMs), since it relies on the representation of the interaction of multi-scale processes, which cannot be reasonably resolved due to the coarse horizontal resolution of RCMs (typically with a gird spacing of 10-50 km) (Kendon et al., 2017; Prein et al., 2015; Gutowski et al., 2020). Some studies found that these RCMs tend to underestimate the frequency of dry days but overestimate the frequency of light rain days (Fowler et al., 2007; Boberg et al., 2009). And significant problems remain with sub-daily statistics in RCMs, for instance, the simulated peak occurs too early and with larger amplitude of diurnal cycle than in observation (Brockhaus et al., 2008; Kendon et al., 2012). Many efforts have been made to accurately predict precipitation, one of the most effective method is to improve the horizontal resolution of RCMs, which has been the development trend of RCMs.

When the resolution of RCMs is increased to convection-permitting (CP) scale, it is possible to switch off the cumulus parameterizations, therefore, CP RCMs are expected to add value than coarser RCMs (Kendon et al., 2012; Prein et al., 2015; Fosser et al., 2015). Many recent results have shown that the spatial distributions of wet day frequency and intensity (Ban et al. 2014; Guo et al., 2019), the diurnal cycle

of precipitation (Fosser et al., 2015; Li et al., 2018; Sun et al., 2016; Guo et al., 2020; Yun et al., 2020) and the duration of extreme hourly precipitation (Kendon et al., 2012; Lind et al., 2016) can be reasonably represented in CP RCMs. In conclusion, these analyses and evaluations are consistently believed that convective precipitation at short temporal and small spatial scales in the CP RCMs provides the significant benefit than in coarse RCMs (Prein et al., 2013, Ban et al., 2014; Fosser et al., 2015). However, these evaluations are primarily based on an Eulerian frame, which is examined at grid cells of the observed and simulated fields, rather than focused on the moving precipitation systems in a Lagrangian frame.

To examine the properties from the viewpoints of the precipitation systems, we need a nontraditional method to track coherent or contiguous regions of grid cells with characteristic attributes of observation and model results. Object-based algorithm has been widely applied to verify the object such as storms (Chang et al., 2016; 2020), cold cloud (Pempel et al., 2017), mesoscale convective systems (MCS) (Fu et al., 2017; Reinares Martínez and Chaboureau, 2018; Chen et al., 2019; Cheeks et al., 2020), and tropical cyclone (Hagos et al., 2013) in short-term simulations at CP scale. Some new results have been discovered by applying this method to CP RCMs, Wang et al. (2019) showed a good agreement with the observation in term of the convective precipitation intensity and size over U.S, but CP RCMs tend to end the convection too soon. And the translation speed of MCSs are underestimated by CP RCMs (Clark et

al. 2014). More importantly, Chang et al. (2020) revealed that the uncertainties of duration and size of precipitation systems are responsible for common wet biases in CP RCMs. Therefore, to better understand the model deficiencies of CP RCMs, we need to complementally evaluate the encompassed full spatial and temporal characteristics of precipitation systems such as duration, size and propagation.

Although some regional climate simulations at CP scales have been conducted over eastern China, most of the verification methods are over the respective grid points of both observation and CP RCMs, such as they mostly focused on the performance of precipitation amount, frequency and intensity (Xiong and Yan, 2013; Li et al., 2018; Yun et al., 2020; Guo et al., 2020). So far, few studies have focused on the climatological characteristics of precipitation systems in a Lagrangian frame over eastern China and their simulation capabilities in CP RCMs. And the disentangle errors in these properties such as occurrence, duration and spatial coverage would be good to understand the underlying source of model deficiencies, which is of vital importance to the radiative budget, water cycle and water resources management over eastern China.

These motivate us to employ object-based algorithm in observation and CP RCMs to investigate the characteristics from the perspective of precipitation systems (1998-2007) over eastern China. Moreover, spectral nudging (SN) has been shown as an

effective method to improve the precipitation features in the coarse horizontal RCMs (Tang et al., 2017; von Storch et al., 2008). Therefore, we also add an experiment using SN in the CP simulation (CP SN), in contrast with the results of without SN (CP NOSN). In this work, we will assess whether CP RCMs are able to simulate characteristics of trajectory, intensity, coverage area and duration, and evaluate the impact of SN on the simulation of the precipitation systems. By analyzing the characteristics of precipitation systems with various duration, our goal is to provide new perspective for improving the precipitation simulation in CP RCMs.

2. Data and Methods

2.1 Model setup and observational data

The Weather Research and Forecasting (WRF) model Version 3.6.1 (Skamarock et al., 2005) is used to downscale the European Centre for Medium-Range Weather Forecast Interim Reanalysis (Dee et al., 2011) to a CP scale over eastern China. Compared to the CP simulation without SN (CP NOSN), we investigate the impact of SN technique on CP simulation (CP SN), in which the SN technique has been conducted on the horizontal wind fields above the boundary layer. Both the CP NOSN and CP SN are run for continuous 10-year (1998-2007) at a grid spacing of 4 km, and the model domain contains 721×721 points in the horizontal and 35 levels in the vertical. More

details on model configuration, such as model spin-up and physical options are consistent with Guo et al. (2020). We compare the model output to the satellite rainfall CMORPH V1.0 dataset (CMORPH for short) (Joyce et al., 2004) with the high spatial resolution of 8 km (at the equator) and 30 min temporal resolution, which has been shown to be suitable for the sub-daily precipitation over eastern China (Chen et al., 2018). The warm-seasons over eastern China are from May to September, and the major rainy seasons are from June to July. Considering the continuity of precipitation systems that are identified and tracked, the MJJASO (May-June-July-August-September-October) season are chosen as validation time period in this work.

2.2 Object-based algorithm

Objected-based algorithm is used to identify and track precipitation systems from the hourly dataset for both CMORPH and CP simulations in an identical manner. Precipitation systems are the same as MCSs, they will go through the birth, development and extinction in the temporal scale, and also involve certain impacted areas in the spatial scale. To identify the precipitation systems in spatiotemporal observed and modeled dataset, we firstly utilize the rain-rate threshold to define the rain cells at single time step, and then the area-overlap algorithm is employed to determine trajectories of the rain cells over different time steps, which has been widely used for tracking the MCSs (Cheeks et al., 2020, Fu et al., 2017),

A precipitation system is defined as a contiguous region with rain-rate larger than 0.1 mm/hr and the area greater than minimum rain-area coverage, which is set to 100 grid points (100×8 km×8 km) for CMORPH and 400 grid points (400×4 km×4 km) for CP simulations. For two successive time steps, if a rain cell overlaps itself by more than 40% of its area, then they are considered as the same precipitation system. If more than two precipitation systems merge, the largest overlapped rain cell belongs to this precipitation system, and the smaller is assumed to end. If one precipitation system splits into more than two systems, we also assign the largest rain cells to the precipitation system and initialize the smaller rain cells at this time step. Tracking is performed on successive hourly dataset until the rain cell area no longer meet the 40% overlapping-area criteria. And then, we will analyze the duration of all precipitation systems, and only consider the systems last more than 3 hours in both the observation and model simulation. We remove the precipitation systems with the limited coverage area and very short lifetime, because this type of system contributes the negligible rainfall. Finally, we marked the detect precipitation systems as system_1, system_2, system_3, ..., system_N, N stands for the number of precipitation systems we detected.

Fig. 1 illustrates the comparison results of precipitation systems identified by our object-based tracking algorithm (d-f) and CMORPH (a-c), taking the identification

and tracking of precipitation systems occurred in July 2006 as an example. Both the splitting (happened over Jiangxi and Anhui provinces, shown in Figs. 1b, e) and merging (occurred over Qinghai and Ningxia provinces, shown in Figs. 1c, f) of precipitation systems have been well captured by our algorithm. Calculating through the multiple examples, our algorithm can detect about 90% of the accumulated precipitation amount in CMORPH at each time step, which indicating the accumulated precipitation amount tracked by our algorithm at each time step is comparable to the amount from CMORPH. And the spatial correlation coefficients between accumulated precipitation detected by our algorithm at each time step and the precipitation in CMORPH are greater than 0.95, which further proves that it is feasible and reasonable to use the object-based algorithm for the precipitation systems tracking.

2.3 Definition of precipitation systems

We characterize precipitation systems with the following metrics:

1) Duration: The period between the ending $[E(k)]$ and beginning $[B(k)]$ of each precipitation event (units: hr), $D(k)=E(k)-B(k)+1, k=1,2,3\ldots N$, where k denotes the precipitation system.

2) Coverage area: The product of the number of grid points at each time step t (denoted as $g(k,t), k=1,2,3\ldots N, t=1,2,3,\ldots D(k)$) and area of the individual grid cell, that is $s(k,t)=g(k,t)\times 8\,km\times 8\,km$ for CMORPH, and $s(k,t)=g(k,t)\times 4\,km\times 4\,km$ for CP simulations (units: km^2).

3) Intensity: The total rainfall average over all grid points at each time step t (denoted as $\int(k,t), k=1,2,3\ldots N, t=1,2,3,\ldots D(k)$, units: mm/hr).

4) Eccentricity: The ratio of minor to major axis lengths of the rain areas at each time steps t (denoted as $\varepsilon(k,t), k=1,2,3\ldots N, t=1,2,3,\ldots D(k)$).

Trajectories represent the movement of the center of precipitation systems, and the center is defined as the location of the maximum rainfall in each precipitation system (denoted as $(cen_{lat}(k), cen_{lon}(k),\ k=1,2,3\ldots N)$. The moving speed of the precipitation system is defined as the distance traveled over the lifetime of precipitation system divided by the duration (denoted as $spd(k), k=1,2,3\ldots N$). Based on the above definitions, the climatological properties of precipitation systems (e.g. intensity, eccentricity, coverage area) can be characterized as the same dimension with duration. The characteristics of the precipitation systems with various durations is to be presented in section 3.2 and 3.3.

3. Results

3.1 Genesis and movement of precipitation systems

All trajectories of precipitation systems from CMORPH, CP NOSN, CP SN and their differences in tacking density are shown in Fig. 2. Overall, total of 68374 trajectories in MAJJSO 1998-2007 is identified from CMORPH, a large number of samples enable us to perform statistically robust analyses. Fig. 2a shows that precipitation systems with the maximum rainfall of more than 10 mm/hr primarily occur over the ocean and along the coast of eastern China. Compared to CMORPH, less trajectories are identified in both CP NOSN and SN (36980 and 38968 respectively, Table 1), which is related to the underestimations of precipitation frequency in CP RCMs (Guo et al., 2019). One of the reasons might be that the thresholds we used have filtered out some precipitation systems, resulting in the fewer trajectories in CP RCMs. Besides, when we upscale the CP RCMs to the same resolution as the CMORPH, the number of trajectories detected from CP RCMs are increased significantly (53776 and 56253, respectively), which is indicating that the less trajectories in CP RCMs are mainly due to the mismatch with the observed horizontal resolution. Moreover, we note that CP RCMs tend to produce maximal rainfall larger than ~10 mm/hr for all precipitation systems (Figs. 2b-c). From Figs. 2d-e we can see that CP RCMs generally overestimate track density by more than 35% over eastern periphery of Tibetan plateau and Yungui Plateau, but underestimate the track density over most eastern

China by up to -40%, which is the same reason that there are less trajectories in CP RCMs. We have to realize that the uncertainties of track density in CP RCMs also may be attributed by the deficiencies of precipitation frequency in CMORPH than in daily precipitation dataset from more than 2400 stations over eastern China (Guo et al., 2019), since it somewhat relies on the rainfall estimation from the IR sensors of geostationary satellite (Joyce et al., 2004).

To investigate the CP RCMs' ability to simulate the more detail characteristics of these trajectories, we further calculate their orientations, which are computed with the angle relative to the east direction. According to the orientation of trajectories, we category them into four groups: i.e. northeastward ($0° \le angle < 90°$), northwestward ($90° \le angle < 180°$), southwestward ($180° \le angle < 270°$) and southeastward ($270° \le angle < 360°$). The occurrence frequency of trajectories in four directions from observation and simulations are represented in Table 1. In the CMORPH, the number of eastward trajectories account to 61.1% of total observed trajectories, in which 31.8% and 29.3% for northeastward and southeastward, respectively. This feature is consistent with that derived from the Advanced Himawari Imager onboard Himawari-8 in Chen et al. (2019). Both CP NOSN and CP SN can generally describe the proportion of the total number of trajectories in four directions, especially for the

eastward trajectories (Table 1). However, due to the less trajectories in CP RCMs, there are some deviations in the genesis frequency simulations of trajectories in four directions. For example, CP RCMs are underestimated the genesis frequency of the westward (including northwestward and southwestward) trajectories, which are mainly generated from India and Indo-China in CMORPH (Figure not shown).

To clearly see where the precipitation systems originated and the moving characteristics, the simulated spatial distribution of genesis frequency and translation speed of all precipitation systems are compared with the observation (Fig. 3). In the CMORPH, precipitation systems mostly generate from the eastern periphery of Tibetan plateau and the eastern coastal region with the frequency of ~19 times or larger (Fig. 3a). The majority of them move eastwards (Fig. 2a, Table 1) with the speed of ~80 km/hr or faster (Fig. 3d). Over the North China Plain and Yangtze-Huaihe River Valley, the frequency of genesis are less (about ~16 times, Fig. 3a) and translating speed of the precipitation systems are slower (~60 km/hr, Fig. 3d), respectively. It is understandable that the motion of precipitation systems is basically related to the horizontal wind speed in the middle troposphere (Figure not shown). On the whole, CP RCMs are able to capture the observed gradient of genesis frequency and moving speed (Figs. 3b-c, e-f). However, they simulate the less frequent of precipitation systems generate especially from North China Plain, Meiyu Region and Sichuan Basin, which is clearly reflecting the model deficiencies (Figs. 3b-c, e-f).

Besides, we surprisingly find that the moving speed of precipitation systems in CP RCMs are slower than that derived from observation, which mainly related to the underestimated motion of steering flow on 500 hPa (Figure not shown). This phenomenon is a little different from the point-to-point matches of model and observation (Guo et al., 2020; Li et al., 2018) and they showed that CP RCMs tend to reproduce the afternoon peaks with earlier shift of 1-2hr than CMORPH (Guo et al., 2020) and rain gauge (Li et al., 2018) over eastern China. By utilizing SN technique in CP RCMs, the simulations of genesis frequency and moving speed over Meiyu Region and Sichuan Basin (Fig. 3c, f) are more consistent with the observation (Fig. 3a, d), especially for northeastward systems (Figure not shown), which mainly due to the reasonable mid-troposphere wind field in CP SN (Figure not shown). We further confirmed that the better agreement of CP SN can be partly be explained by the use of SN method to large-scale flow patterns, which is consistent with the simulating results of Tang et al. (2017) at coarser resolution of RCMs.

3.2 Statistics of precipitation systems duration

Table 2 summarizes the properties of precipitation systems derived from CMORPH and CP NOSN and SN. Although the number of precipitation systems identified from CP RCMs is fewer than that in CMORPH, the average intensity of precipitation systems simulated by CP RCMs (3.2 mm/hr, +77.8%) is significantly stronger than

301 those in CMORPH (1.8 mm/hr). This is consistent with the previous studies based on
302 the point-to-point validation (Yun et al., 2020; Guo et al., 2020; Li et al., 2018).
303 Comparing to the point-to-point validation, the object-based algorithm enables us to
304 evaluate the ability of CP RCMs in simulating the duration and shape of precipitation
305 systems. From Table 2, we can see that the average duration and eccentricity of
306 precipitation systems can be well simulated in CP NOSN and CP SN, and only
307 increase slightly by about +1.1% (8.9 hr) and +1.2% (0.85) compared with CMORPH
308 (8.8 hr and 0.84). However, the uncertainties of average coverage area in CP NOSN
309 (23241km^2) and CP SN (22314 km^2) are obviously decreased by -10.6% and -14.0%,
310 respectively. Compared to CP NOSN, CP SN tends to have a smaller coverage area,
311 which may be due to the constraint of large-scale atmospheric circulations in RCMs
312 on the convective development (Tang et al., 2017; von Storch et al., 2008).

313

314 The characteristics of intensity and coverage area of objects, such as MCSs and
315 storms, are commonly illustrated by their probability and cumulative frequency
316 distributions (PDF, CDF) or the scatterplots in the literature (Davis et al., 2006a, b;
317 Clark et al., 2014; Li et al., 2020; Cheeks et al., 2020; Pempel et al., 2017; Prein et al.,
318 2013). However, to see more clearly the uncertainties of coverage area and intensity
319 in CP RCMs, the density-scatter plots of coverage-area-duration, intensity-duration
320 and eccentricity-duration are shown in Fig. 4. In the CMORPH, the shorter-duration (

321 ¿$48\,hr$) systems occur frequently, but the coverage area beyond $200 \times 10^3\,km^2$ are

322 extremely rare (Fig. 4a). In addition, the observed shape of intensity-duration just like
323 skewed distribution (Fig. 4d). These features can be well simulated by CP RCMs, but
324 the simulated density-scatter distributions of coverage-area-duration are excessive
325 concentrated (Figs. 4b-c), and the intensity-duration are more dispersed (Figs. 4e-f).
326 We note that there are significant deviations in the simulations of intensity and
327 coverage area of precipitation systems with shorter-duration. To be more specific, the
328 coverage-area-duration distribution of shorter-duration precipitation systems tend to
329 be less dense in both CP NOSN and SN (Figs. 4b and 4c), which corresponds to the
330 underestimations of coverage area in CP RCMs (Table 2). Figs. 4e-f also show the
331 simulated intensity-duration distribution is wider along the intensity axis than that in
332 CMORPH, especially for the systems shorter-duration. This implies that CP RCMs
333 tend to overestimate the intensity of precipitation systems (Table 2, Fig.7 b).
334 However, Figs. 4h-j indicate that the density-scatter of eccentricity-duration in CP
335 NOSN and CP SN are visually not distinguishable from the CMORPH, indicating that
336 CP RCMs have abilities to reproduce the reasonable spatial distribution accumulated
337 amount of precipitation systems.

338

339 CP RCMs can not only accurately simulate the averaged properties of precipitation
340 systems, but also the dependence of intensity on coverage area, which has been shown
341 more important than the values themselves (Davis et al. 2006b). Figure 5 displays the

relationship between mean intensity and mean maximal rainfall and coverage area for all precipitation systems (Figs. 5a, d), shorter-duration precipitation systems (Figs. 5b, e) and longer-duration ($\geq 48\,hr$) precipitation systems (Figs. 5c, f). Due to the frequent occurrence of shorter-duration systems (Fig. 4), there are similar features between the shorter-duration systems (Fig. 5b, e) and all precipitation systems (Fig. 5a, d) in CMORPH. Both the observed intensity and maximal rainfall increase along with the expansion of the precipitation system when the coverage area is within $150 \times 10^3\,km^2$, and show steady constants afterward (Fig. 5a, b, d and e). But for the longer-duration systems, both the intensity and maximal rainfall are almost constant in CMORPH. These observed features changing with the coverage area for longer-duration systems can be well described by CP RCMs. However, for the shorter-duration systems, the significant decreasing of mean intensity and maximal rainfall in CP RCMs are completely contrary to those in the observation (Fig. 5a, b, d and e), especially for smaller coverage area. And this may be because that CP RCMs tend to reproduce more intense and localized precipitation systems, which is causing the uncertainties of intensity and coverage areas in CP RCMs. Clearly, CP SN shows substantial improvements over CP NOSN, it can reduce the intensity and maximal rainfall biases.

3.3 Contribution to precipitation amount

The spatial distribution of the accumulated precipitation amount (APA) of all systems,

362 shorter-duration systems and longer-duration systems are given in Fig. 6, and the
363 spatial correlation coefficients (CORs) and root mean square errors (RMSEs) between
364 simulations and observation are listed in Table 3. The large value of observed APA of
365 all systems mainly appears in the Yangtze-Huaihe River Valley and South China with
366 the magnitude over 9 cm/year (Fig. 6a). For the shorter-duration systems in
367 CMORPH, the APA of shorter-duration systems also occurs at the southeastern
368 periphery of Tibetan plateau and the southern coastal China with maximal amount
369 over 7cm/year (Fig. 6d). But for the longer-duration systems, the observed maximal
370 accumulated amount (over 5cm/year) primarily locates along the southeast coastal
371 areas (Fig. 6g). CP RCMs properly simulate the decline of all systems' APA from
372 southeast to northwest, so that the spatial CORs between CP RCMs and CMORPH
373 are 0.78 and 0.80, respectively (Figs. 6b-c, Table 3). It can be found that both CP
374 NOSN and CP SN underestimate the all APA over Mei-yu Region and Southern
375 China, but they overestimate the APA over the area surrounding Sichuan Basin and
376 Yungui Plateau (Figs. 6b-c). Moreover, it is obvious that CP RCMs have dry biases
377 for shorter-duration precipitation systems, but have wet biases for the longer-duration
378 APA (Figs. 6d-f and Figs. 6g-i), which is partly related to the overestimation of
379 maximal intensity shown in Figs. 2a-c. Comparing to CP NOSN, the encouraging
380 results of shorter-duration, longer-duration systems are seen in the CP SN with the
381 higher CORs and the least RMSEs (Table 3).

382

We further divide the shorter-duration and longer-duration precipitation systems into nine classes (A-I) according to their durations (Table 3). From the spatial distributions of APA for the nine-classes (Figure not shown) and the associated statistics listed in Table 3. As we expected, CP RCMs can properly represent the APA of precipitation with duration less than 24 hr (Class A-C) with CORs above 0.72 (Table 3). However, we find that CP RCMs have relatively poor simulation of the precipitation systems lasting from 24 hr to 96 hr (class D-F), which mainly occur over eastern periphery of Tibetan plateau (Figure not shown). Surprisingly, we note that CP RCMs have potential capability to capture the precipitation with duration longer than 120 hours (class H-I) (with CORs above 0.68 and small RMSEs), which also can be seen in Figs. 4 and 5. From the spatial COR and RMSEs of the nine-classes systems, we further confirm that the CP SN achieve notable added value for the precipitation amount than CP NOSN.

To verify what causes the APA of precipitation systems with different durations in CP RCMs, the statistics of the occurrence frequency, contribution to the total precipitation amount, the average intensity and coverage area for the nine-class precipitation systems (class A-I) are comparatively presented in Fig. 7. Consistent with the results using traditional verification and results shown in Fig. 4, we find that the observed shorter-duration systems occur frequently (98.8%; Fig.7a). However, this type of systems only account for 63.7% of total precipitation amount in

CMORPH (Fig .7b). The longer-duration systems remain certain contributions to total precipitation amount, although they rarely occur (Fig. 7b). From Figs. 7c-d, we can see that the observed average intensity of systems does not varies notably (Fig. 7c) while both the observed coverage area (Fig. 7d) changes significantly as the duration increases, which resulting in the contributions to total precipitation amount changes with duration (Fig. 7b). But for simulations in CP RCMs, the relationship between the average intensity/coverage area/total precipitation amount and duration are different between CP RCMs and CMORPH (Figs. 7 c-d). It can be found that the underestimations of the contribution of total precipitation amount for the shorter-duration systems (class A-D) are caused by the combination with the consistent occurrence frequency and coverage areas changing. While the overestimations of the contribution of total precipitation amount for the longer-duration systems (E-I) are in line with the changing of intensity in CP RCM.

More importantly, we note that the contributions to the total precipitation amount for shorter-duration and longer-duration systems in CP NOSN and CP SN are resulting in different reasons. By using SN in CP RCM makes more significant contribution to the total precipitation amount for shorter-duration systems than that in CP NOSN (Fig. 7b), which is in line with the different intensity variations shown in CP RCMs (Fig. 7c). Therefore, we infer that the different shorter-duration precipitation amount between in CP NOSN and CP SN are caused by the bias of intensity. But the different

longer-duration precipitation amount in CP NOSN and CP SN are consistent with their different coverage areas. For example, he class G makes bigger contribution to the total precipitation amount in CP SN than that in CP NOSN, which corresponds to the larger coverage area in CP SN than that in CP NOSN. Such a corresponding relation can also be found in classes E, F, H and I.

Summary and Conclusions

Object-based algorithm has been applied to identify and track precipitation systems from both observation and CP RCMs over eastern China during the period 1998-2007. The climatological characteristics of precipitation systems such as genesis frequency, translation speed, duration, coverage area and intensity have been investigated in this work. The evaluation of these properties in CP RCMs complements the previous studies that only considered the spatial dimension alone or focused on the case studies. Furthermore, the improving ability of SN technique of CP RCM is analyzed by comparing without SN. Our findings are summarized below.

For the genesis frequency and trajectories of precipitation systems, we emphasize the spatial matching between CP RCMs and CMORPH. Although CP RCMs produce less precipitation systems than CMORPH, the genesis locations and propagations of the

precipitation systems are properly captured in the CP RCMs. The precipitation systems in CP RCMs are more frequently generated from the eastern periphery of Tibetan plateau and Yungui Plateau. And thus, CP RCMs have more track density over there, which may be responsible for the overestimations of precipitation amount in those regions. Consistent with Clark et al., 2014, the moving velocity of precipitation systems are significant slower in CP RCMs than in observation. However, this phenomenon is different from the results of the traditional point-to-point matching of observations and the CP simulations over eastern China, in which the afternoon diurnal peak of precipitation tend to be earlier in CP RCMs (Li et al., 2018; Guo et al., 2020; Yun et al., 2020). Since deep convective precipitation systems usually occurred in the afternoon over eastern China (Yu et al., 2010), which is indicated that the moving speed of convective precipitation systems in CP RCMs tend to be faster, while the speed of non-convective precipitation systems in CP RCMs tend to be slower. Moreover, we further separate these trajectories into four categories (northeastward, northwestward, southwestward and southeastward), it is found that the simulated occurrence frequency of the precipitation systems in the four groups are closer as observation. However, the moving speed in the four groups are underestimated in CP RCMs, especially for the northeastward and southeastward, and these deficiencies of the moving speed in the four groups can be made up by employing SN method in CP RCMs.

With regards to the climatological properties of precipitation systems over eastern China, CP RCMs describe the duration and eccentricity of the systems appropriately, while large simulating biases are found in the systems' intensity and coverage area. Compared to CMORPH, the model-simulated density-scatter distributions of coverage-area-duration and the intensity-duration are more concentrated and wider, respectively, which corresponds the underestimation of coverage area and over-prediction of intensity in CP RCMs. The analysis on the relationships between intensity/maximum rainfall and coverage area of the precipitation systems indicates that CP RCMs are able to capture the general functional relationships, especially for the longer-duration systems (≥48hr). However, for both shorter-duration (¿48hr) and longer-duration systems, the intensity derived from CP RCMs is usually too strong when the systems' coverage area is relatively small. The sensitivity experiment with SN shows that SN technique in CP RCMs can be helpful to reduce the biases in intensity and maximal rainfall of all precipitation systems.

In terms of the accumulated precipitation amount, CP RCMs can satisfactorily simulate the spatial distribution of total precipitation, however, dry and wet biases in shorter-duration and longer-duration systems have found in CP RCMs, respectively. By employing SN method in CP RCMs will revise these bias and have better performance their spatial distributions due to the less root mean square error and higher spatial correlation coefficient than without SN. The added value of CP SN than

CP NOSN is reconfirmed by analyzing the accumulated precipitation amount of nine groups (class A-I), which are classified according to the duration of precipitation systems. Furthermore, the different contributions to total precipitation amount between CP NOSN and SN are revealed, for the longer-duration systems (class E-I), the different contributions between CP SN and CP NOSN are primarily resulted from their differences in coverage area. Nevertheless, for the shorter-duration systems, CP SN contributes more to the total precipitation amount than CP NOSN, which are related to the more intense precipitation in CP SN.

Overall, the climatology characteristics of precipitation systems over eastern China can be reasonably captured in CP RCMs. However, from the perspective of precipitation systems, the simulated intensity and coverage area in CP RCMs tend to be stronger and smaller, respectively. And wet biases and dry biases for shorter-duration and longer-duration systems have been shown in CP RCMs. These deficiencies of CP RCMs need to be further improved, for example, we could improve the simulations of precipitation systems' intensity and coverage areas since they are virtually important factors for precipitation amount deviations in CP RCMs. More importantly, we need to improve the relationship between intensity and coverage area, especially for the locally isolated precipitation systems with shorter-duration.

It is worthy of noting that the analyses performed in this work are based on the object-

based tracking method. On the whole, the object-based tracking algorithm is an efficient and objective method for tracking precipitation systems. This is why the object-based method is widely used for tracking supercells, mesoscale convective systems, tropical cyclones, heat waves and so on. However, there are some issues about this method that needs to be acknowledged or discussed. Although both the rain-rate threshold and area-threshold may arouse some uncertainties, it doesn't make any difference to our conclusion. For example, too many tests have been performed by increasing the area-threshold from 100-200 grid points (100×8 km×8 km-200×8 km×8 km) for CMORPH and 400-800 grid points (400×8 km×8 km-800×8 km×8 km) for CP simulations, respectively. Albeit the occurrence frequency of precipitation systems will decrease, the overestimations of intensity and underestimations of coverage area are also existed. Moreover, it is noted that this method only can provide the time-domain characteristics of individual systems, but without the spatial distribution of systems. Along with the development of the CP RCMs, the case-based evaluations on the simulations of CP RCMs will be more important in the analysis on the added value of CP RCMs. The more efficient and reasonable object-based tracking will do great help to such investigations.

Acknowledgments

National Key Research and Development Program of China (2018YFA0606003) and the National Natural Science Foundation of China (41875124, 41875067) jointly fund this work. The numerical calculations in this paper have been done on the computing facilities in the High Performance Computing Center (HPCC) of Nanjing University. The authors also acknowledge with thanks the ECMWF for providing the ERA-interim reanalysis data as driving fields in the simulations, and NOAA's Climate Precipitation Center (CPC) for providing the CMORPH observational data, which is available at ftp://ftp.cpc.ncep.noaa.gov/precip/CMORPH_V1.0/CRT/ . We declare that we have no conflict of interest.

Reference

Ban, N., Schmidli, J., & Schär, C. (2014). Evaluation of the convection− resolving regional climate modelling approach in decade− long simulations. Journal of Geophysical Research: Atmospheres, 119, 7889–7907. https://doi.org/10.1002/2014JD021478.

Boberg, F., P. Berg, P. Thejll, W.J. Gutowski, and J.H.Christensen, (2009). Improved confidence in climate change projections of precipitation evaluated using daily statistics from the PRUDENCE ensemble. Climate Dyn., 32, 1097–1106.

Brockhaus, P., D. Lu¨thi, and C. Scha¨r, 2008: Aspects of the diurnal cycle in a regional climate model. Meteor. Z., 17, 433–443.

Chang W, Stein ML, Wang J, Kotamarthi VR, Moyer EJ (2016) Changes in spatiotemporal precipitation patterns in changing climate conditions. J Clim 29(23):8355–8376.

Chang, W., Wang, J., Marohnic, J. et al. Diagnosing added value of convection-permitting regional models using precipitation event identification and tracking. Clim Dyn 55, 175–192 (2020). https://doi.org/10.1007/s00382-018-4294-0.

Cheeks, S. M., S. Fueglistaler, and S. T. Garner, 2020: A Satellite-Based Climatology of Central and Southeastern U.S. Mesoscale Convective Systems. Mon. Wea. Rev., 148, 2607–2621, https://doi.org/10.1175/MWR-D-20-0027.1.

Chen G, Lan R, Zeng W, Pan H, Li W (2018) Diurnal variations of rainfall in surface and satellite observations at the monsoon coast (South China). J Clim 31(5):1703–1724.

Chen, D., Guo, J., Yao, D., Lin, Y., Zhao, C., Min, M., et al. (2019). Mesoscale convective systems in the Asian monsoon region from Advanced Himawari Imager: Algorithms and preliminary results. Journal of Geophysical Research: Atmospheres, 124, 2210–2234. https://doi.org/10.1029/2018JD029707.

Clark AJ, Bullock RG, Jensen TL, Xue M, Kong F (2014) Application of object-based time-domain diagnostics for tracking precipitation systems in convection-allowing models. Weather Forecast 29(3):517–542.

Davis, C., B. Brown, and R. Bullock, 2006a: Object-based verification of precipitation forecasts. Part I: Methodology and application to mesoscale rain areas. Mon. Wea. Rev., 134, 1772–1784, doi:10.1175/MWR3145.1.

Davis, C., B. Brown, and R. Bullock, 2006b: Object-based verification of precipitation forecasts. Part II: Application to convective rain systems. Mon. Wea. Rev., 134, 1785–1795, doi:10.1175/MWR3146.1.

Dee DP, Uppala SM, Simmons AJ, Berrisford P, Poli P, Kobayashi Set al (2011) The ERA-Interim reanalysis: configuration and performance of the data assimilation system. Q J R Meteorol Soc 137(656):553–597.

Fosser G, Khodayar S, Berg P (2015). Benefit of convection permitting climate model simulations in the representation of convective precipitation. Climate Dynamics, 44(1-2), 45-60.

Fowler, H. J., S. Blenkinsop, and A. P. Smith, (2007). Estimating change in extreme European precipitation using a multimodel ensemble. J. Geophys. Res., 112, D18104, doi:10.1029/2007JD008619.

Fu, S., J. Sun, Y. Luo, and Y. Zhang, 2017: Formation of Long-Lived Summertime Mesoscale Vortices over Central East China:Semi-Idealized Simulations Based on a 14-Year Vortex Statistic. J. Atmos. Sci., 74, 3955–3979, https://doi.org/10.1175/JAS-D-16-0328.1.

Guo, Z., Fang, J., Sun, X. et al. Decadal long convection-permitting regional climate simulations over eastern China: evaluation of diurnal cycle of precipitation. Clim Dyn 54, 1329–1349 (2020). https://doi.org/10.1007/s00382-019-05061-z

Guo, Z., Fang, J., Sun, X., Yang, Y., & Tang, J. (2019). Sensitivity of summer precipitation simulation to microphysics parameterization over eastern China: Convection−permitting regional climate simulation. Journal of Geophysical Research: Atmospheres, 124. https://doi.org/10.1029/2019JD030295.

Gutowski W J , Ullrich P A , Hall A , et al. The Ongoing Need for High-Resolution Regional Climate Models: Process Understanding and Stakeholder Information[J]. Bulletin of the American Meteorological Society, 2020, 101(5).

Hagos, S., Z. Feng, S. McFarlane, and L. R. Leung, 2013: Environment and the Lifetime of Tropical Deep Convection in a Cloud-Permitting Regional Model Simulation. J. Atmos. Sci., 70, 2409–2425, https://doi.org/10.1175/JAS-D-12-0260.1.

Joyce, R. J., Janowiak, J. E., Arkin, P. A., & Xie, P. (2004). Cmorph: a method that produces global precipitation estimates from passive microwave and infrared data at high spatial and temporal resolution. Journal of Hydrometeorology, 5(3), 287-296.

Kendon, E. J., Roberts, N. M., Senior, C. A., & Roberts, M. J. (2012). Realism of rainfall in a very high-resolution regional climate model. Journal of Climate, 25(17), 5791-5806.

Kendon, E. J., Ban, N., Roberts, N. M., Fowler, H. J., Roberts, M. J., Chan, S. C., Evans, J. P., Fosser, G., & Wilkinson, J. M. (2017). Do Convection-Permitting Regional Climate Models Improve Projections of Future Precipitation Change?, Bulletin of the American Meteorological Society, 98(1), 79-93. Retrieved Jan 21, 2021,

from https://journals.ametsoc.org/view/journals/bams/98/1/bams-d-15-0004.1.xml
Li, P., Furtado, K., Zhou, T., Chen, H., Li, J., Guo, Z., & Xiao, C. (2018) The diurnal cycle of East Asian summer monsoon precipitation simulated by the Met Office Unified Model at convection-permitting scales. Climate Dynamics, 1-21.
Li, Z., Y. Luo, Y. Du, and J. C. L. Chan, 2020: Statistical characteristics of pre-summer rainfall over South China and associated synoptic conditions. J. Meteor. Soc. Japan, 98, 213–233, doi:10.2151/jmsj.2020-012.
Lind, P., Lindstedt, D., Kjellström, E., & Jones, C. (2016). Spatial and temporal characteristics of summer precipitation over central Europe in a suite of high-resolution climate models. Journal of Climate, 29(10), 3501-3518.
Prein A F, Langhans W, Fosser G, et al. (2015). A review on regional convection−permitting climate modeling: Demonstrations, prospects, and challenges. Reviews of geophysics, 53(2): 323-361.
Reinares Martínez, I., and J. Chaboureau, 2018: Precipitation and Mesoscale Convective Systems: Explicit versus Parameterized Convection over Northern Africa. Mon. Wea. Rev., 146, 797–812, https://doi.org/10.1175/MWR-D-17-0202.1.
Rempel, M., F. Senf, and H. Deneke, 2017: Object-Based Metrics for Forecast Verification of Convective Development with Geostationary Satellite Data. Mon. Wea. Rev., 145, 3161–3178, https://doi.org/10.1175/MWR-D-16-0480.1.
Skamarock, W. C., J. B. Klemp, J. Dudhia, D. O. Gill, D. M. Barker, M. G. Duda, X. Huang, W. Wang, and J. G. Powers (2008), A description of the advanced research WRF version 3, NCAR Tech. Note, NCAR/TN-475 + STR, 8 pp., Natl. Cent. for Atmos. Res., Boulder, Colo. [Available at http://www.mmm.ucar. edu/wrf/users/docs/arw619 v3.pdf, 2008.]
Sun, X., M. Xue, J. Brotzge, R. A.McPherson, X.-M. Hu, and X.-Q. Yang (2016), An evaluation of dynamical downscaling of Central Plains summer precipitation using a WRF-based regional climate model at a convection-permitting 4 km resolution, J. Geophys. Res. Atmos., 121, 13,801–13,825, doi:10.1002/2016JD024796.
Tang, J. , Wang, S. , Niu, X. , Hui, P. , Zong, P. , & Wang, X. . (2017). Impact of spectral nudging on regional climate simulation over cordex east asia using wrf. Climate dynamics, 48(7-8), 2339-2357.
von Storch H, Langenberg H, Feser F. A spectral nudging technique for dynamical downscaling purposes[J]. Monthly weather review, 2000, 128(10): 3664-3673.
Wang, J., X. Dong, A. Kennedy, B. Hagenhoff, and B. Xi, 2019: A Regime-Based Evaluation of Southern and Northern Great Plains Warm-Season Precipitation Events in WRF. Wea. Forecasting, 34, 805–831, https://doi.org/10.1175/WAF-D-19-0025.1.
Xiong, Z., and Yan, X. (2013), Building a high-resolution regional climate model for the Heihe River Basin and simulating precipitation over this region. Chinese science bulletin, 58(36), 4670-4678.
Yun, Y. , Liu, C. , Luo, Y. , Liang, X. , Huang, L. , & Chen, F. , et al. (2020). Convection-permitting regional climate simulation of warm-season precipitation over eastern china. Climate Dynamics, 54(3), 1469-1489.

Table and Figure Captions

Table 1 Comparisons of the occurrence frequency of the trajectories in four directions from CMORPH, CP NOSN and SN. Numbers in brackets represent the contribution (%) relative to the total trajectories for CMORPH, CP NOSN, CP SN, respectively.

Table 2 Comparisons of the properties of precipitation systems in CMORPH, CP NOSN and SN. Numbers in brackets represent the differences (%) relative to CMORPH.

Table 3. The spatial COR RMSE of accumulated precipitation amount for systems with different durations between CMORPH and CP NOSN and CP SN.

Fig. 1 An example for identifying and tracking the precipitation systems occurred from 0200 UTC to 0400 UTC 2 July 2006. Precipitation derived from CMORPH (a-c) and identified precipitation systems represented by the same color at each time step (d-f).

Fig. 2 Tracks of precipitation systems derived from CMORPH (a), CP NOSN (b) and CP SN (c) in MJJASO 1998-2007. Colors of the tracks correspond to the systems' maximum rainfall. Track density differences (d-e) between model and observation, which are binned to 0.5°×0.5° grid spacing. The black solid lines outlined North China Plain (107°–122° E, 32°– 41° N), Mei-yu Region (112°–122° E, 27°– 32° N), Southern China (110°–120° E, 22°– 27° N), Sichuan Basin (103°–108° E, 28°– 32° N) and Yungui Plateau (102°–110° E, 22°– 28° N), respectively.

Fig. 3 Spatial distribution of the genesis density (a-c) and the moving speed (d-f) of precipitation

systems as identified and tracked from CMORPH, CP NOSN and CP SN in MJJASO 1998-2007. Note that the genesis density and moving speed are binned to 0.5°×0.5°grid spacing. The sub-regions are outlined by black lines as shown in Fig. 2.

Fig. 4 Density-scatter plot of the object coverage area (a-c), intensity (d-f), eccentricity (h-j) and duration from CMORPH, CP NOSN and CP SN in MJJASO 1998-2007, the black dotted lines are represented by objects with duration of 48 hr.

Fig. 5 The mean intensity and mean maximal rainfall as a function of coverage area for all systems (a, d), shorter-duration systems (b, e) and longer-duration systems (c, f) from CMORPH, CP NOSN and CP SN in MJJASO 1998-2007.

Fig 6. The spatial distribution of total precipitation amount for all systems (a-c), shorter-duration (d-f), longer-duration systems (g-i) detected from CMORPH, CP NOSN and CP SN in MJJASO 1998-2007. The sub-regions are outlined by black lines as shown in Fig. 2.

Fig 7. Histograms of the occurrence frequency (a) of nine categories classified by different duration and their contributions (b) to total amount, and box-and-whisker plots of the average intensity (c) and coverage area (d) for nine categories from CMORPH, CP NOSN and CP SN in MJJASO 1998-2007.

Table 1 Comparisons of the occurrence frequency of the trajectories in four directions from CMORPH, CP NOSN and SN. Numbers in brackets represent the contribution (%) relative to the total trajectories for CMORPH, CP NOSN, CP SN, respectively.

Movement Direction	Occurrence Frequency		
	CMORPH	CP NOSN	CP SN
Northeastward	21709 [31.8%]	11883 [32.1%]	12985[33.3%]
Northwestward	9466 [13.8%]	7485 [20.2%]	7172[18.4%]
Southwestward	17136[25.7%]	7914[21.4%]	8160[20.9%]
Southeastward	20063[29.3%]	9698[26.3%]	10651[27.4%]
Total trajectories	68374	36980	38968

Table 2 Comparisons of the properties of precipitation systems in CMORPH, CP NOSN and SN. Numbers in brackets represent the differences (%) relative to CMORPH.

	CMORPH	CP NOSN	CP SN

Average duration of systems (hr)	8.8	8.9 [+1.1%]	8.9 [+1.1%]
Average intensity of hourly rainfall (mm/hr)	1.8	3.2 [+77.8%]	3.2 [+77.8%]
Average coverage area of systems (km^2)	25986	23241 [-10.6%]	22314 [-14.0%]
Average eccentricity of systems	0.84	0.85 [+1.2%]	0.85 [+1.2%]

713
714
715
716
717

718 **Table 3.** The spatial COR RMSE of accumulated precipitation amount for systems with different
719 durations between CMORPH and CP NOSN and CP SN.

Duration		CP NOSN		CP SN	
		COR	RMSE	COR	RMSE
3-6hr (Class A)		0.74	2.24	0.75	2.50
6-12hr (Class B)		0.76	3.23	0.76	3.23
12-24hr (Class C)		0.72	6.32	0.72	6.40
24-48hr (Class D)		0.43	7.62	0.48	7.61
Total	3-48hr	0.74	1.38	0.77	1.36
Total	>=48hr	0.68	17.3	0.78	12.8
48-72hr (Class E)		0.39	5.68	0.46	5.16
72-96hr (Class F)		0.31	4.65	0.55	3.50
96-120hr (Class G)		0.56	4.91	0.66	4.91
120-144hr (Class H)		0.68	3.71	0.81	2.08
>=144hr (Class I)		0.77	4.54	0.80	3.13
All		0.78	20.4	0.80	18.8

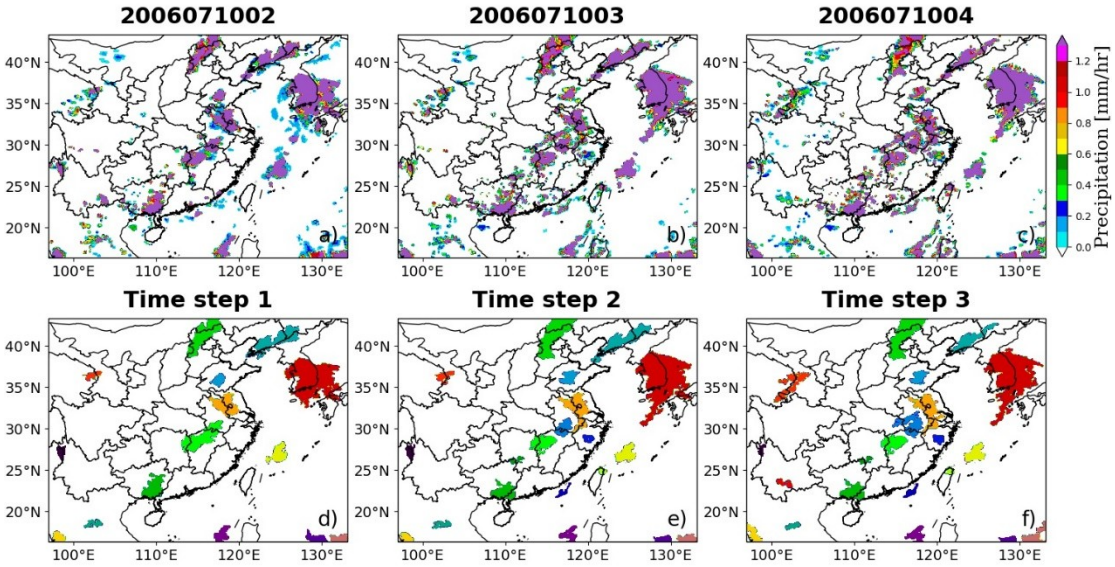

720

721 **Fig. 1** An example for identifying and tracking the precipitation systems occurred from 0200 UTC

63
64

to 0400 UTC 2 July 2006. Precipitation derived from CMORPH (a-c) and identified precipitation systems represented by the same color at each time step (d-f).

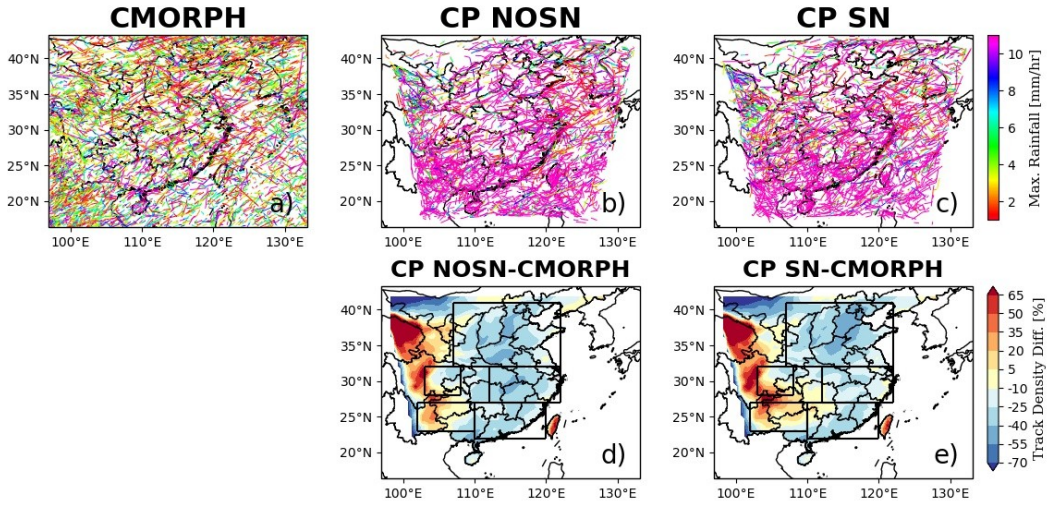

Fig. 2 Tracks of precipitation systems derived from CMORPH (a), CP NOSN (b) and CP SN (c) in MJJASO 1998-2007. Colors of the tracks correspond to the systems' maximum rainfall. Track density differences (d-e) between model and observation, which are binned to 0.5°×0.5° grid spacing. The black solid lines outlined North China Plain (107°–122° E, 32°– 41° N), Mei-yu Region (112°–122° E, 27°– 32° N), Southern China (110°–120° E, 22°– 27° N), Sichuan Basin

(103°–108° E, 28°– 32° N) and Yungui Plateau (102°–110° E, 22°– 28° N), respectively.

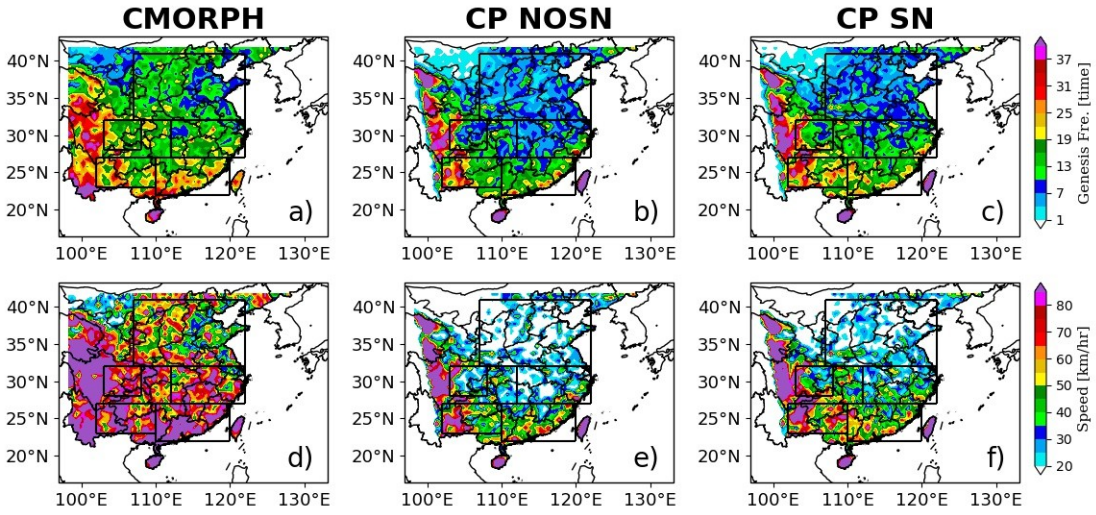

Fig. 3 Spatial distribution of the genesis density (a-c) and the moving speed (d-f) of precipitation systems as identified and tracked from CMORPH, CP NOSN and CP SN in MJJASO 1998-2007. Note that the genesis density and moving speed are binned to 0.5°×0.5°grid spacing. The sub-regions are outlined by black lines as shown in Fig. 2.

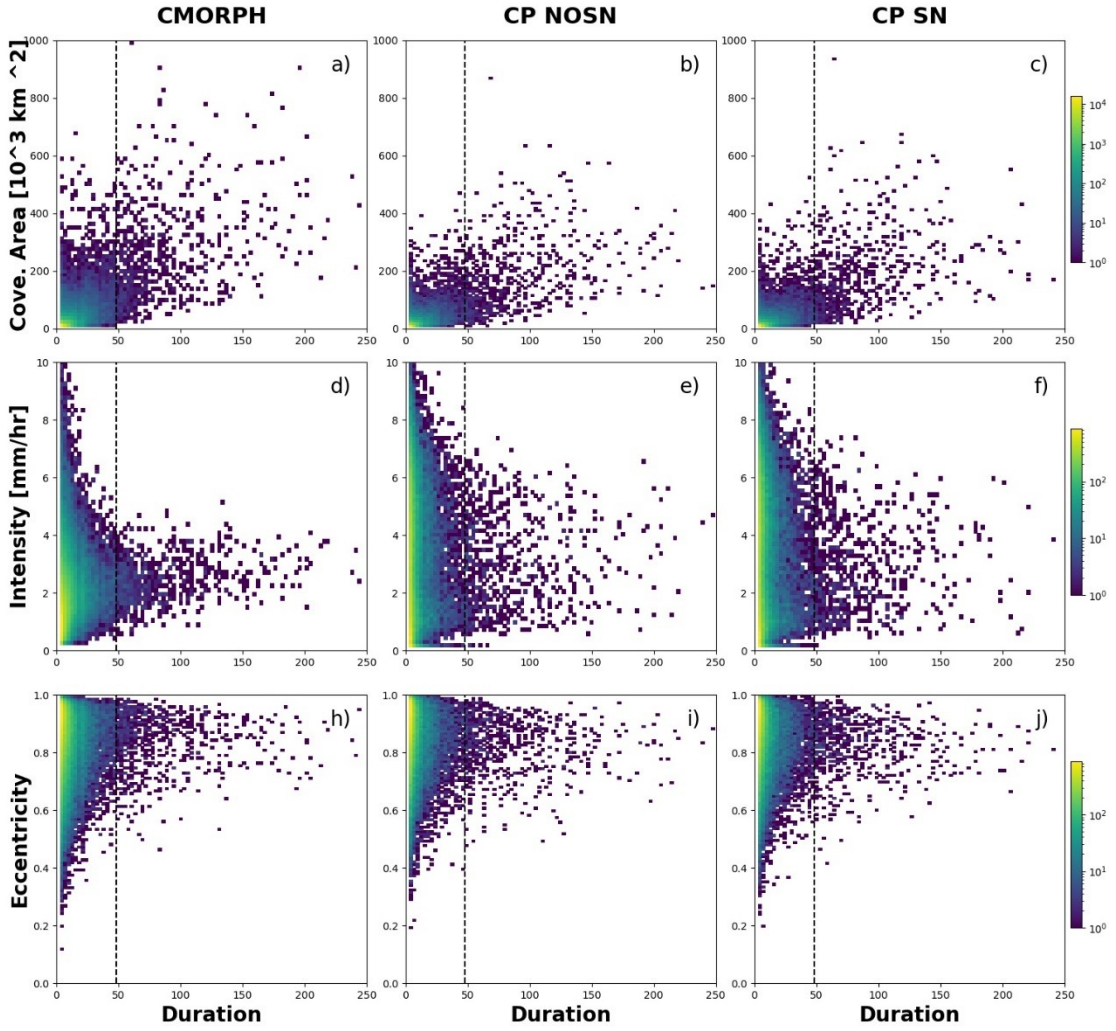

Fig. 4 Density-scatter plot of the object coverage area (a-c), intensity (d-f), eccentricity (h-j) and duration from CMORPH, CP NOSN and CP SN in MJJASO 1998-2007, the black dotted lines are represented by objects with duration of 48 hr.

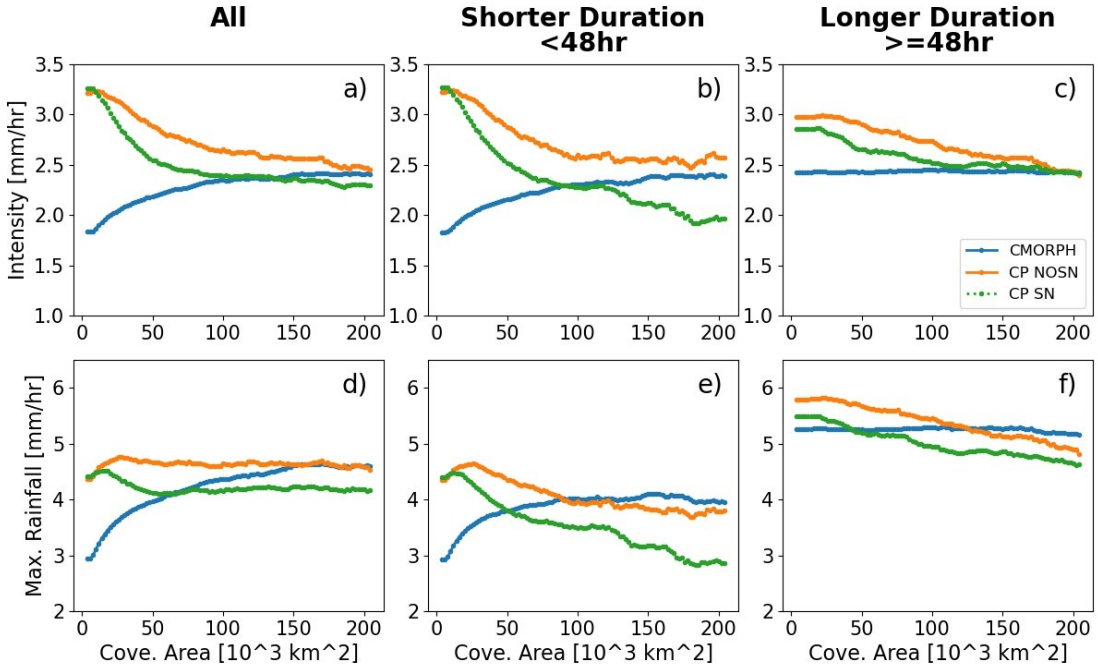

Fig. 5 The mean intensity and mean maximal rainfall as a function of coverage area for all systems (a, d), shorter-duration systems (b, e) and longer-duration systems (c, f) from CMORPH, CP NOSN and CP SN in MJJASO 1998-2007.

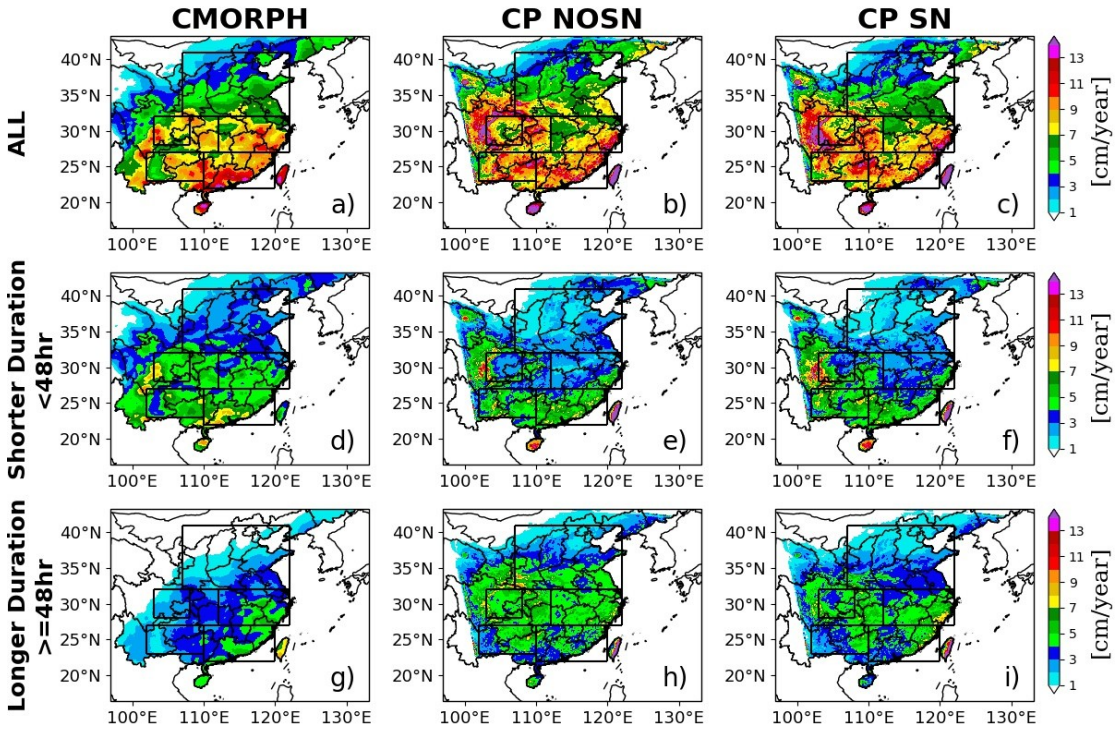

Fig 6. The spatial distribution of total precipitation amount for all systems (a-c), shorter-duration (d-f), longer-duration systems (g-i) detected from CMORPH, CP NOSN and CP SN in MJJASO 1998-2007. The sub-regions are outlined by black lines as shown in Fig. 2.

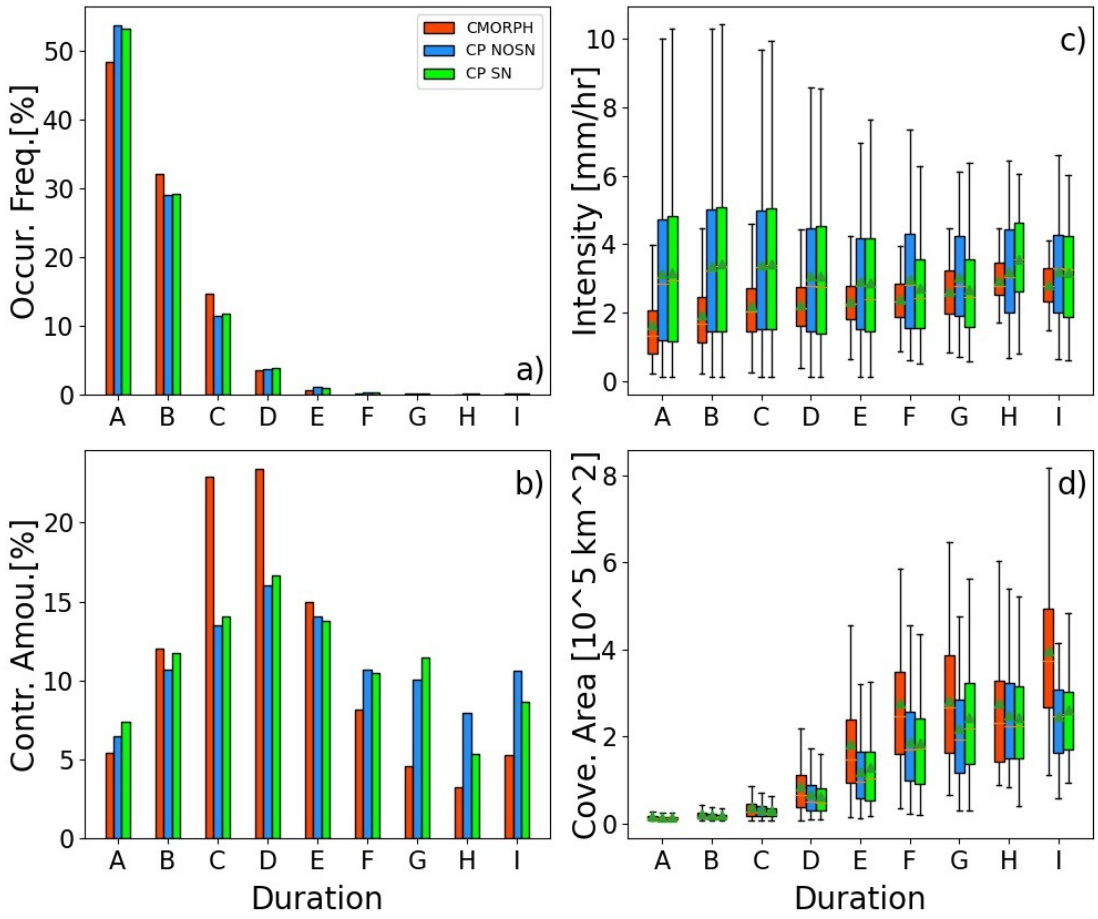

886

887 **Fig 7.** Histograms of the occurrence frequency (a) of nine categories classified by different
888 duration and their contributions (b) to total amount, and box-and-whisker plots of the average
889 intensity (c) and coverage area (d) for nine categories from CMORPH, CP NOSN and CP SN in
890 MJJASO 1998-2007.